AFRL-RW-EG-TR-2013-079

SIMULATING THE RESONANT ACOUSTIC MIXER

Douglas V. Nance

AFRL/RWWC
101 W. Eglin Blvd.
Eglin AFB, FL 32542-6810

AUGUST 2013

INTERIM REPORT

AIR FORCE RESEARCH LABORATORY
MUNITIONS DIRECTORATE

■ **Air Force Materiel Command** ■ **United States Air Force** ■ **Eglin Air Force Base, FL 32542**

NOTICE AND SIGNATURE PAGE

Using Government drawings, specifications, or other data included in this document for any purpose other than Government procurement does not in any obligate the U.S. Government. The fact that the Government formulated or supplied the drawings, specifications, or other data does not license the holder or any other person or corporation, or convey any rights or permission to manufacture, use, or sell any patented invention that may relate to them.

This report was cleared for public release by the 96th Air Base Wing, Public Affairs Office, and is available to the general public, including foreign nationals. Copies may be obtained from the Defense Technical Information Center (DTIC) < http://www.dtic.mil/dtic/index/html>.

AFRL-RW-EG-TR-2013-079 HAS BEEN REVIEWED AND IS APPROVED FOR PUBLICATION IN ACCORDANCE WITH ASSIGNED DISTRIBUTION STATEMENT.

FOR THE DIRECTOR:

Signed	Signed
Craig M. Ewing, DR-IV, Ph.D. Munition Systems Effects Sciences CTC Lead Weapon Engagement Division	Douglas V. Nance, Ph.D. Research Scientist AFRL/RWWC

This report is published in the interest of scientific and technical information exchange, and its publication does not constitute the Government's approval or disapproval of its ideas or findings.

REPORT DOCUMENTATION PAGE

Form Approved
OMB No. 0704-0188

PLEASE DO NOT RETURN YOUR FORM TO THE ABOVE ADDRESS.

1. REPORT DATE *(DD-MM-YYYY)*	2. REPORT TYPE	3. DATES COVERED *(From - To)*
02-08-2013	INTERIM	15-05-2013 - 02-08-2013

4. TITLE AND SUBTITLE

SIMULATING THE RESONANT ACOUSTIC MIXER

5a. CONTRACT NUMBER

5b. GRANT NUMBER

5c. PROGRAM ELEMENT NUMBER

62602F

6. AUTHOR(S)

Douglas V. Nance

5d. PROJECT NUMBER

2502

5e. TASK NUMBER

67

5f. WORK UNIT NUMBER

63

7. PERFORMING ORGANIZATION NAME(S) AND ADDRESS(ES)

AFRL/RWWC
101 W. Eglin Blvd.
Eglin AFB, FL 32542-6810

8. PERFORMING ORGANIZATION REPORT NUMBER

AFRL-RW-EG-TR-2013-079

9. SPONSORING/MONITORING AGENCY NAME(S) AND ADDRESS(ES)

AFRL/RWMES
101 W. Eglin Blvd.
Eglin AFB, FL 32542-6810

10. SPONSOR/MONITOR'S ACRONYM(S)

AFRL-RW-EG-TR

11. SPONSOR/MONITOR'S REPORT NUMBER(S)

AFRL-RW-EG-TR-2013-079

12. DISTRIBUTION/AVAILABILITY STATEMENT

Distribution A: Approved for public release: distribution unlimited. (96ABW-2013-0221, 23 July 2013)

13. SUPPLEMENTARY NOTES

14. ABSTRACT

This report utilizes a state-of-the-art multiphase physics computer code to develop a rationale and a procedure for simulating the fluid dynamics of the Resonant Acoustic Mixer. This type of mixer does not require the use of blades to create high shear in the mixable medium. Rather it uses acoustic vibrations to couple vorticity and pressure fluctuations to create small mixing zones throughout the sample. This report uses computational fluid dynamics to study the mixer's physics. Two mixing test problems are solved, one for a mixture of Oxygen and Nitrogen, a second for a two high viscosity materials. Results are presented for each case, and additional research is planned and documented.

15. SUBJECT TERMS

acoustic, mixer, MacCormack, viscosity, fluctuation, vorticity, resin

16. SECURITY CLASSIFICATION OF:			17. LIMITATION OF ABSTRACT	18. NUMBER OF PAGES	19a. NAME OF RESPONSIBLE PERSON
a. REPORT	b. ABSTRACT	c. THIS PAGE			D. Nance
UNCLAS	UNCLAS	UNCLAS	UL	27	19b. TELEPHONE NUMBER *(Include area code)*

Reset

TABLE OF CONTENTS

Section **Page**

LIST OF FIGURES

1.0 INTRODUCTION

The process of mixing is an interesting fluid dynamical phenomenon possessing a wide range of industrial applications. Many materials used by society rely upon the formation of mixtures of constituent "purer" materials. For instance, concrete is a mixture formed from sand, water, aggregate (rock) and dry concrete powder. The latter material is itself a mixture of solid particulate materials. Also, even more common applications of mixing are found in the food service industry since many common foods are mixtures, e.g., soups, sauces, cereals, soft drinks and many, many others. In order to achieve a level of industrial efficiency, we must endeavor to understand the mixing process since mechanical energy is consumed by mixing. At the industrial scale, an inefficient mixing process slows the process of combining of ingredients and adds to the required mixing time. This inefficiency increases the cost of mixing; hence, it raises the price of the product. In other ways, mixing may create undesirable effects on the material such as temperature excursions and void formation. High shear mixing can easily cause fluid cavitation, the sudden formation and catastrophic collapse of tiny voids. This process consumes valuable energy and raises the fluid temperature. It also generates noise. When creating mixtures of energetic materials, it is, in most cases, necessary to prevent these mixing-related phenomena from occurring. High shear mixing can also damage many fluids such as human blood and enzymes like insulin (by either breaking or folding chemical chains).

High shear mixing is a common mixing process of some familiarity to nearly everyone. It is the process employed by household cake mixers. Arrays of metal or plastic blades are rotated through the material in question. The basic property of viscosity requires that there be no velocity difference between the blade surface and the fluid. As a result, the fluid adjacent to the blade surface is dragged along with the blade causing shear. The layer of fluid at the blade surface moves at a different speed than adjacent fluid layers creating a shear layer. This layer tends to roll up with adjacent fluid layers, a phenomenon that typifies the mixing process. The roll up of the layer places thin regions of different materials together. Repetition combines material layers over ever smaller scales making for thorough or more complete mixing. High shear mixing is effective and simple, but it does engender some deleterious side effects. The action of viscosity leads to friction that dissipates mechanical energy into heat. In certain cases, the material being mixed may reach high temperatures. For energetic materials, this heating is not welcome. Also, for complex biological fluids, mixing can cause the formation of material "strands" that change the mechanical properties of the fluid. In these cases, it is beneficial to employ an alternative mixing process, one that does not rely on direct material shear.

Resonant Acoustic Mixing (RAM) is a process that employs acoustic waves, at a relatively low frequency (60 Hz), to drive the mixing process.[1] In RAM, the fluid and vessel are envisioned as a spring-mass-damper system where energy is transferred between the springs and the moving fluid masses. A condition of resonance is sought where acoustic energy from a driving source is directed into the kinetic energy of fluid eddies. The purpose of the present work is to determine whether or not some aspects of this process can be captured by high fidelity numerical simulation, i.e., by solving the Navier-Stokes equations. This project is interesting because the resonance condition sought in [1] is related to a linear, second order ordinary differential equation whereas the Navier-Stokes equations are inherently nonlinear through the participation of the advective terms for fluid motion.[2] Questions also arise in the context of the

type of mixing encountered. Turbulent fluid motions tend to result in the most effective mixing because the turbulent cascade of energy tends to direct energy into smaller and smaller scales of motion. That is to say, fully developed turbulence is characterized by the generation of ever smaller sized eddies (regions of circulating fluid). The direct interpretation of this process is that ever smaller masses of fluid are combined together; hence, more effective mixing occurs. Yet, turbulence is generally confined to high Reynolds number flow fields, those flow fields where inertial forces tend to dominate over viscous forces. Viscous forces tend to dissipate or regularize fluid motion toward laminar flow. For these reasons, turbulence is not likely to occur for high viscosity mixing. Still, even at high viscosities, this fact does not preclude organized rotational or unstable fluid motion. Purely hydrodynamic instabilities such as Rayleigh-Taylor and Richtmyer-Meshkov instabilities also occur.[3] These phenomena are true fluid instabilities that do not possess some of the physical features of turbulence such as randomness and intermittency.[4] Yet, these instabilities may support highly efficient mixing.

The discussions that follow constitute only a beginner's investigation of acoustic mixing. Much of the data associated with commercial RAM is likely to be of a proprietary nature and not available to the individuals outside of the Resonant Acoustic Mixers corporation. The mixer documentation indicates that the acoustic excitation is truly based in physical vibration of the sample (instead of actual sound) with a fundamental frequency of 60 Hz.[1] Yet, the mixer design professes to have the ability to sense conditions of resonance and adjust the excitation accordingly. The studies shown below do use true acoustic excitation with fixed amplitude and at the fundamental frequency. The fluid dynamics are genuine as predicted by numerical solutions of the Navier-Stokes equations calculated by using the Large Eddy Simulation with LInear Eddy modeling in 3 Dimensions (LESLIE3D) multiphase physics computer program. LESLIE3D is developed cooperatively by the Air Force Research Laboratory and Professor Suresh Menon at the Georgia Institute of Technology. Hands-on development of this computer code is accomplished by staff at Professor Suresh Menon's Computational Combustion Laboratory.

2.0 METHODS, ASSUMPTIONS AND PROCEDURES

In the manner of review, sound or acoustic radiation is a longitudinal compression-rarefaction wave. In most cases, these waves travel as weak (linear) disturbances in a gas, liquid or solid material medium. Every isotropic medium at constant thermodynamic conditions has a fixed speed of sound (or celerity), and this speed is the maximum possible propagation speed for a weak or linear disturbance. Although not routinely encountered, there are cases where strong acoustic waves exhibit nonlinear behavior.[5] This phenomenon does occur in regions near the tips of turbo-machinery blades. Common acoustic waves retain linear character and may be superposed. In spite of their linear behavior, the propagation of sound waves in moving media is accurately modeled by the Navier-Stokes equations. These equations admit solutions for both linear and nonlinear waves for all speed regimes where the medium is modeled as a continuum. This system of equations is solved by LESLIE3D, so we begin our theoretical discussion with a presentation of these equations.

2.1 Navier-Stokes Equations

The Navier-Stokes equations constitute a system of conservation laws for mass, momentum and energy (when expressed in homogeneous form).[6] For problems involving multiple phases (such as a dispersed phase of particles), the equations become nonhomogeneous. The overall system still retains conservative behavior but recognizes the presence of mass, momentum and energy "sources". The present work involves no dispersed phase. In Cartesian coordinates, the conservation of mass equation may be written as

$$\frac{\partial \rho}{\partial t} + \frac{\partial (\rho u_j)}{\partial x_j} = 0 \tag{1}$$

with the summation convention in effect. The conservation of momentum is enforced by the following equation.

$$\frac{\partial (\rho u_i)}{\partial t} + \frac{\partial (\rho u_i u_j + \delta_{ij} P - \tau_{ij})}{\partial x_j} = 0 \quad i = 1, \ldots, 3 \tag{2}$$

where the stress tensor τ_{ij} is defined as

$$\tau_{ij} = \lambda \delta_{ij} \frac{\partial u_k}{\partial x_k} + \mu \left(\frac{\partial u_i}{\partial x_j} + \frac{\partial u_j}{\partial x_i} \right) \tag{3}$$

Coefficient μ is the dynamic viscosity while λ is a parameter put forth by Stokes to represent the effect of dilatational stress.[2] By Stoke's hypothesis, this factor is normally taken as

$$\lambda = -\tfrac{2}{3} \mu \tag{4}$$

It follows that the first term in (3) is the dilatational stress while the second term is the shear stress. The conservation of energy equation is expressed in a similar form, i.e.,

$$\frac{\partial(\rho E)}{\partial t}+\frac{\partial[(\rho E+P)u_j-\tau_{ij}u_i+q_j]}{\partial x_j}=0 \tag{5}$$

where

$$q_j=-K\frac{\partial T}{\partial x_j} \tag{6}$$

represents the components of the heat conduction vector within the fluid (Fourier's Law). In (5), we have also introduced the total energy per unit mass E, i.e.,

$$E=e+\tfrac{1}{2}u_k u_k \tag{7}$$

This system of conservation laws is not mathematically closed. In order to achieve closure, we must add a sixth equation, namely the equation of state. The equation of state, in most cases and for pure, single phase substances, is a relation that relates three thermodynamic variables. A frequently encountered form for gases is

$$P=P(\rho,e) \tag{8}$$

For the configurations discussed in this report, we employ a special form of (8) commonly known as the perfect gas equation of state.

$$P=\rho R\,T \tag{9}$$

The simulations conducted here exist at an early stage in research, so (9) is applied in the calorically perfect manifestation where

$$R=C_p-C_v \tag{10}$$

$$e=C_v T \tag{11}$$

$$\gamma=C_p/C_v \tag{12}$$

C_p and C_v are both constant for the calorically perfect gas model.[6] For chemically reacting flow fields, a set of species equations are included within the system. The species equations may be expressed as

$$\frac{\partial(\rho Y_m)}{\partial t}+\frac{\partial[\rho Y_m(u_j+V_{jm})]}{\partial x_j}=\dot{\omega}_m \tag{13}$$

For a flow field containing *N* species, the mass fractions are constrained so that

$$\sum_{m=1}^{N} Y_m = 1 \tag{14}$$

The diffusion velocity components are defined as

$$V_{im} = -\frac{D_m}{Y_m}\frac{\partial Y_m}{\partial x_i} \tag{15}$$

with the constraint (summation convention does not apply to *m*)

$$\sum_{m=1}^{N} V_{im} = 0 \tag{16}$$

For multi-species flow fields, the internal energy has an alternative expression from that shown in (11). Based upon species enthalpies we have that

$$e = \sum_{m=1}^{N} Y_m h_m - \frac{P}{\rho} \tag{17}$$

where

$$h_m = \Delta h_{fm}^0 + \int_{T_0}^{T} C_{pm}(\tilde{T})\, d\tilde{T} \tag{18}$$

2.2 Navier-Stokes Equations in Dimensionless Form

One may often derive great insight for a physical problem by considering the pertinent governing equations in dimensionless form. This assertion is particularly true for the Navier-Stokes equations. One may remove the dimensions from these equations by replacing the dimensioned variables occurring in the equations with a set of scaled, dimensionless variables. The fluid dynamical variables may be scaled as follows.

$$\begin{aligned} x_i &= L\,\tilde{x}_i \qquad & t &= T\,\tilde{t} \\ u_i &= {}^{L}\!\!\diagup\!\!_{T}\ \tilde{u}_i = u_0\,u_i \qquad & \rho &= \rho_0\,\tilde{\rho} \end{aligned} \tag{19}$$

where *L*, *T*, *L/T* and ρ_0 are the length, time, velocity and density scales for the problem. In the momentum equation, pressure must be scaled, so the consistent units for pressure are

$$[P] = [\rho u_0^2] = \rho_0 (L/T)^2 \tag{20}$$

Also, in the scope of dimensional analysis, (7) provides the scale for energy, i.e.,

$$[E]=[u^2]=(L/T)^2 \tag{21}$$

Hence,

$$P=\rho_0 (L/T)^2 \,\tilde{P}; \quad E=(L/T)^2 \,\tilde{E} \tag{22}$$

Absolute temperature requires a slightly different treatment; informally for calorically perfect gases, we may write that

$$E=C_p \Theta \tag{23}$$

By asserting that

$$\Theta=\Theta_o \tilde{\Theta} \tag{24}$$

we can apply (22) and show that

$$\Theta_0=\frac{(L/T)^2}{C_p} \tag{25}$$

By using (3) and (19), we can show that

$$\frac{\partial \tau_{ij}}{\partial x_j}=\frac{\mu}{LT}\frac{\partial \tilde{\tau}_{ij}}{\partial \tilde{x}_j} \tag{26}$$

and that

$$\frac{\partial (\tau_{ij} u_i)}{\partial x_j}=\frac{\mu}{T^2}\frac{\partial (\tilde{\tau}_{ij}\,\tilde{u}_i)}{\partial \tilde{x}_j} \tag{27}$$

$$\frac{\partial q_j}{\partial x_j}=-\frac{K}{C_p T^2} \tag{28}$$

By using (19), we can write the dimensionless continuity equation as

$$\frac{\partial \tilde{\rho}}{\partial \tilde{t}}+\frac{\partial (\tilde{\rho}\,\tilde{u}_j)}{\partial x_j}=0 \tag{29}$$

The application of (19) and (26) to (2) leads to the dimensionless momentum equation

$$\frac{\partial(\tilde{\rho}\,\tilde{u}_i)}{\partial\tilde{t}} + \frac{\partial(\tilde{\rho}\tilde{u}_i\tilde{u}_j + \delta_{ij}\tilde{P}-)}{\partial\tilde{x}_j} = \frac{1}{\mathrm{Re}}\frac{\partial\tilde{\tau}_{ij}}{\partial\tilde{x}_j} \quad i = 1,\ 2, 3 \tag{30}$$

where the Reynolds number, Re, is defined as

$$\mathrm{Re} = \frac{\rho_0\, u_0\, L}{\mu} \tag{31}$$

Similarly, equations (19), (27) and (28) may be used to convert (5) into the dimensionless energy equation

$$\frac{\partial(\tilde{\rho}\,\tilde{E})}{\partial\tilde{t}} + \frac{\partial[(\tilde{\rho}\,\tilde{E} + \tilde{P})\tilde{u}_j]}{\partial\tilde{x}_j} = \frac{1}{\mathrm{Re}}\frac{\partial(\tilde{\tau}_{ij}\,\tilde{u}_i)}{\partial\tilde{x}_j} - \frac{1}{\mathrm{Re}\,\mathrm{Pr}}\frac{\partial\tilde{q}_j}{\partial\tilde{x}_j} \tag{32}$$

In (32), the Prandlt number, Pr, is defined as

$$\mathrm{Pr} = \frac{\mu C_p}{k} \tag{33}$$

Both the Reynolds and Prandtl numbers are dimensionless quantities that are strongly related to the properties of a compressible, viscous flow field. The Reynolds number represents the ratio of inertial to viscous forces. On the other hand, the Prandtl number conveys the ratio of the flow field's ability to transport momentum to its ability to transport heat.[2] These dimensionless numbers (or groups) are drawn from the mathematical theory of similarity, a system of powerful techniques useful for solving a wide array of problems in physics.[7] As it relates to fluid flow problems such as the RAM, we can say that two different flow fields that possess the same geometry (streamline configuration) and the same Reynolds and Prandtl numbers are *similar* for slow speed (Mach zero) flows. That is to say, their flow solutions map onto one another through the use of the scaling system discussed above.

For the RAM problem, dimensionless groups are important, particularly the Reynolds number. The extent of mixing is, in part, dictated by the scales of shear motion in a given flow field. The widest division of shear motion scales is encountered in turbulent flow fields, and turbulence thus provides the most efficient mixing. Yet, the level of turbulence is closely associated with the Reynolds number. It is interesting that the amount of data available for the RAM permits that an estimate of the Reynolds number be made. These calculations are shown later in Sections 3.1 and 3.2. The target problem, mixing at high values of dynamic viscosity, presents an interesting departure for LESLIE3D. The first reason for this departure is straightforward; we are trying to simulate either a liquid-liquid of liquid-solid mixing problem by using a multiphase gas dynamics code. The second reason is of equal interest. LESLIE3D is designed for the dynamic large eddy simulation of turbulence. High viscosity mixing, in this case, is confined to low Reynolds numbers; hence, it is unlikely to involve turbulence. As a result, LESLIE3D is operated in direct numerical simulation (DNS) mode for laminar mixing.

For LESLIE3D, this territory is unexplored. Part of the knowledge to be gained from working on this problem is how to operate the computer code for this class of mixing problem. We also hope to determining the limitations of using this approach.

2.3 Vector Forms for the Finite Volume Method

LESLIE3D is programmed to solve multiphase flow problems with descriptive units. That is to say, every property is expressed in an appropriate system of units. By default, the meter-kilogram-second (MKS) system is employed by the computer code. As a result, LESLIE3D applies the governing equations in dimensional form as shown in Section 2.1 To numerically solve this system, we may place the system in vector form to facilitate its solution via the finite volume method.[6] Since the system (1-13) is cast in conservative form (with source terms), this process is not difficult. Note that we do not admit the presence of chemical reactions (nor of mass sources). The vector Navier-Stokes equations for multi-species flow may be written as

$$\frac{\partial \mathbf{U}}{\partial t}+\frac{\partial \mathbf{F}}{\partial x}+\frac{\partial \mathbf{G}}{\partial y}+\frac{\partial \mathbf{H}}{\partial z}=0 \tag{34}$$

where the vector of conserved variables is given by

$$\mathbf{U}=(\rho,\,\rho u,\,\rho v,\,\rho w,\rho E,\,\rho Y_n)^T \tag{35}$$

The remaining terms in (34) are Cartesian derivatives of the flux vectors (for *n* species), i.e.,

$$\mathbf{F}=\begin{bmatrix}\rho u,\,\rho u^2+P-\tau_{xx},\rho uv-\tau_{xy},\,\rho uw-\tau_{xz},\\ u(\rho E+P)-u\tau_{xx}-v\tau_{xy}-w\tau_{xz}+q_x,\,\rho Y_n\left(u+V_{xn}\dfrac{\partial Y_n}{\partial x}\right)\end{bmatrix}^T \tag{36}$$

$$\mathbf{G}=\begin{bmatrix}\rho v,\,\rho vu-\tau_{yx},\rho v^2+P-\tau_{yy},\,\rho vw-\tau_{yz},\\ v(\rho E+P)-u\tau_{yx}-v\tau_{yy}-w\tau_{yz}+q_y,\,\rho Y_n\left(v+V_{yn}\dfrac{\partial Y_n}{\partial y}\right)\end{bmatrix}^T \tag{37}$$

$$\mathbf{H}=\begin{bmatrix}\rho w,\,\rho wu-\tau_{zx},\rho wv-\tau_{zy},\,\rho w^2+P-\tau_{zz},\\ w(\rho E+P)-u\tau_{zx}-v\tau_{zy}-w\tau_{zz}+q_z,\,\rho Y_n\left(w+V_n\dfrac{\partial Y_n}{\partial z}\right)\end{bmatrix}^T \tag{38}$$

Equation (34) has a very special form. Let us denote

$$\mathbf{A}=\hat{i}\mathbf{F}+\hat{j}\mathbf{G}+\hat{k}\mathbf{H} \tag{39}$$

then (34) becomes

$$\frac{\partial \mathbf{U}}{\partial t} + \nabla \bullet \mathbf{A} = 0 \tag{40}$$

Let us integrate (40) in space over a hexahedral control volume such as the one shown in Figure 1. Doing so is a key step for this discretization method. The integration is annotated as follows.

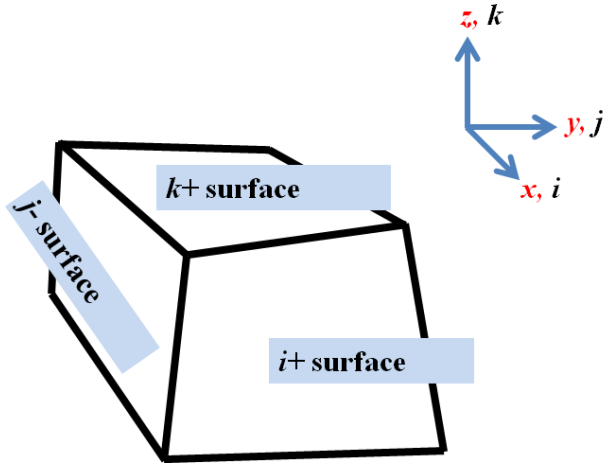

Figure 1. Hexahedral control volume (volume V) for the finite volume method

$$\frac{d}{dt}\int_V \mathbf{U} d\upsilon + \int_V \nabla \bullet \mathbf{A} d\upsilon = 0 \tag{41}$$

Application of the divergence theorem yields

$$\frac{d}{dt}\int_V \mathbf{U} d\upsilon + \oint_{B(V)} \mathbf{A} \bullet \hat{n} = 0 \tag{42}$$

Note that in both (41) and (42), the time derivative is now ordinary. All of the spatial dependence of its argument has been removed by integration. The right hand term has been transformed into an integral computed over a closed surface. For the hexahedral volume shown in Figure 1, this integral is evaluated as the sum of surface integrals computed over the six sides of the control volume, i.e.,

$$\frac{d}{dt}\int_V \mathbf{U} d\upsilon + \sum_{m=1}^{6} \mathbf{A} \bullet \hat{n}_m \Delta s_m = 0 \tag{43}$$

Equation (43) is a semi-discrete form that can be integrated by the same algorithms used for solving ordinary differential equations. The fully explicit Multi-step Runge-Kutta methods offer a great deal of utility in solving this type of equation in time.[9] The right hand term addresses that dependence of the fluid system on space. It contains several space derivatives, particularly for the physics of viscosity, heat conduction and molecular diffusion. From the standpoint of pragmatics, this method completely separates the algorithms for temporal and spatial discretization. If we center the discretization on the cell indexed by (i, j, k), we can evaluate the volume integral by $\tilde{\mathbf{U}}$ (an averaged value for $\mathbf{U}$ theoretically existing at the cell center) multiplied by the cell volume. The current version of LESLIE3D utilizes structured grids, so the

right hand term in (43) (a sum of flux vectors) possesses an underlying order. The flux vectors are oriented along three curvilinear directions delineated by ordinal indices *i*, *j* and *k*. As a result, this term can be written as the differences in flux computed along these directions. The time derivative may be evaluated by using a general Newton divided difference. With these qualifications, (43) can be rewritten as

$$\frac{\delta \tilde{\mathbf{U}}^{n}_{i,j,k}}{\Delta t} V_{i,j,k} = -\sum_{i=1}^{3} \left[(\mathbf{A} \bullet \hat{n}_i^{+}) \Delta s_i^{+} - (\mathbf{A} \bullet \hat{n}_i^{-}) \Delta s_i^{-} \right] = -\sum_{i=1}^{3} (f_i^{+} - f_i^{-}) \tag{44}$$

In (44), index *i* represents the three directions *i*, *j* and *k* on the grid. The + and – signs represent the sign of the flux given by its cell face as is shown in Figure 1. This structured grid approach permits the computationally efficient form existing on the right side of (44). This form illustrates that the change in properties within a cell is determined by the difference in flux across the cell. Several discretization schemes may be applied to (44), but the present work is concentrated on applying MacCormack's method.[10]

2.4 MacCormack Discretization

MacCormack's method is a classic predictor-corrector scheme. The predictor step uses information available at the current time level to produce a solution estimate at an "intermediate" time level. The estimate at this step possesses an error that is biased in the forward space direction. The corrector step uses information at both the current and intermediate time levels to estimate the solution at the new time level. In the calculation of this step, error is biased in the backward space direction. The strength of this method is that by reversing the sign of error generation at each step, the new growth of numerical error is maintained small. In the notation of (44), the predictor step is written as

$$\tilde{\mathbf{U}}^{*}_{i,j,k} = \tilde{\mathbf{U}}^{n}_{i,j,k} - \frac{\Delta t}{V_{i,j,k}} \left[(f^{+(n)}_{i+1/2,j,k} - f^{+(n)}_{i-1/2,j,k}) + (f^{+(n)}_{i,j+1/2,k} - f^{+(n)}_{i,j-1/2,k}) + (f^{+(n)}_{i,j,k+1/2} - f^{+(n)}_{i,j,k-1/2}) \right] \tag{45}$$

whereas the corrector step is written as

$$\begin{aligned} \tilde{\mathbf{U}}^{n+1}_{i,j,k} &= \tfrac{1}{2} (\tilde{\mathbf{U}}^{n}_{i,j,k} + \tilde{\mathbf{U}}^{*}_{i,j,k}) \\ &\quad - \frac{\Delta t}{2V_{i,j,k}} \left[(f^{-(*)}_{i+1/2,j,k} - f^{-(*)}_{i-1/2,j,k}) + (f^{-(*)}_{i,j+1/2,k} - f^{-(*)}_{i,j-1/2,k}) + (f^{-(*)}_{i,j,k+1/2} - f^{-(*)}_{i,j,k-1/2}) \right] \end{aligned} \tag{46}$$

The half-index notation used in (45) and (46) allows flexibility in setting the formal order of accuracy for the flux calculation.[6] As an example, a second order MacCormack scheme may be constructed by assigning

$$f^{+(n)}_{i+1/2,j,k} = f^{(n)}_{i+1,j,k} \; ; \quad f^{-(n)}_{i+1/2,j,k} = f^{(n)}_{i,j,k} \tag{47}$$

with similar expressions for directions *j* and *k*. The problems addressed in the results section apply the second order MacCormack scheme is pure form with no artificial viscosity. Hence, the attendant solutions form a baseline case for more in-depth simulations to be performed later.

2.5 Boundary Conditions

When solving partial differential equations, boundary conditions frequently become an issue of contention due to the difficulties associated with the proper representation of physics at the boundary. Significant numerical theory is often required to create reasonably good boundary conditions. Fortunately, the configurations considered in this work involve only solid surface boundaries. The exception to this rule is the boundary where acoustic forcing is implemented. The set-up of this condition is discussed in the next section. Otherwise, solid surface boundaries are enforced through the use of the first adjacent ghost cell. The details are omitted, but both slip and no-slip boundaries are easily treated by the processes described in Hirsch [6] or Poinsot and Lele.[11]

2.6 Acoustic Forcing

The RAM mixes materials by exploiting the coupling that can occur between acoustic pressure (or velocity) fluctuations with fluctuating vorticity. Adjacent "layers" of fluid are wrapped together by circulating fluid loops established by the rotation existing in vortices. Viscosity is an important contributor to this process since it makes the fluid layers "adhere" to one another. Acoustic forcing must be expressed in an algorithmic form that can be incorporated in LESLIE3D. Specifically, this algorithm is established within a solid surface boundary routine that sets ghost (or phantom) cell values for the boundary where excitation is employed. Forcing is applied as a perturbation added to main flow values of pressure and velocity.[8] Consistent values of ghost cell density and internal energy are then calculated to complete the update. The manifestation of acoustic excitation applied for this report is described as follows. We assume that the acoustic pressure has fixed amplitude and angular frequency, i.e.,

$$P_{ac} = 0.1 P_{atm} \sin(2\pi\omega t) \tag{34}$$

The magnitude of pressure forcing may be adjusted by changing the "0.1" in (34) to some other value. Yet, this magnitude may be kept small to ensure that the perturbation does not exceed the acoustic level. The accompanying velocity perturbation is calculated from the equation

$$v_{ac} = \frac{P_{ac}}{\rho c} \tag{35}$$

where ρ and c are calculated in the flow field cell immediately adjacent to the wall.[8] The acoustic pressure perturbation is added to the flow field pressure found in the boundary adjacent flow field cell and then stored in the ghost cell. The acoustic velocity perturbation is added to the flow field velocity normal to the boundary and stored similarly. Internal and total energies for the ghost cell are then computed as discussed in Section 2.1. In essence, this algorithm is a good representation for the situation where an acoustic wave enters the flow field at this boundary.

However, RAM acoustic forcing seems more mechanical in nature. That is to say, the mixing canister is essential shaken at a frequency of about 60 Hz. This condition is more difficult to represent in terms of a boundary condition algorithm since the entire container is shaken on a platform. Still, the algorithm described above is suitable for initial estimates.

3.0 RESULTS

In this report, we simulate the physics for two notional problems where mixing is driven by continuous wave acoustic excitation. While both test problems employ a cylindrical mixing vessel, the first problem involves the mixing of Nitrogen and Oxygen gases. The equations of state and transport algorithms built into LESLIE3D are well suited for solving this problem. This problem lends insight into the basic physics of mixing. The second problem presents a far greater challenge for LESLIE3D. In this case, we employ high viscosity fluids that, in truth, should be modeled by the use of a liquid equation of state. However, we also treat these fluids as gases in order to minimize required changes to the computer program. The attendant viscosities are very high therefore increasing the natural damping in the system and weakening the acoustic waves.

3.1 Oxygen – Nitrogen Mixing

LESLIE3D possesses transport data (temperature dependent viscosity and thermal conductivity data) for both Oxygen and Nitrogen. As perfect gases, these substances are well understood, so their mixture defines an excellent test case for the new acoustic excitation algorithm. This problem is designed to execute as a multi-block problem using 25 blocks or subdomains. The geometry is that of a cylinder one meter in diameter with a height of 3 meters. The block structure and initial gas concentration plots are shown in Figure 2.

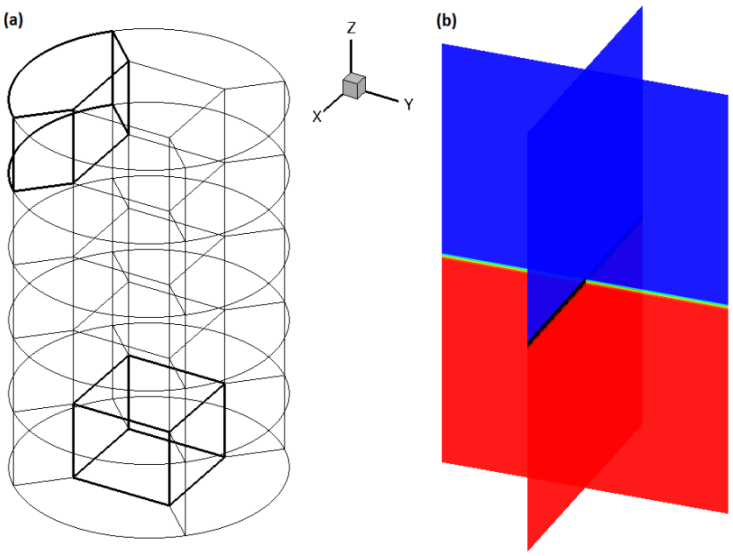

Figure 2. Set-up of the Oxygen-Nitrogen mixing test problem.

Figure 2(a) presents the block structure. The mixer is cut into a set of thick disks along the *z* axis. Each disk is then divided into five hexahedral regions. The center block is box-shaped while the remaining four regions have the same shape with a circular outer boundary. Each block has the same volume and the same number of cells and grid points. Figure 2(b) offers a simple

view of the initial mass fractions for species Nitrogen and Oxygen. This plots shows two slices cut through the flow field, one parallel to the *xz*-plane and one parallel to the *yz*-plane. The blue color represents Nitrogen; red indicates pure Oxygen. Colors intermediate between blue and red indicate a mixture of the two. As is indicated by the figure, the Nitrogen mass is situated atop the Oxygen bubble. There is no gravity in this simulation. No-slip boundary conditions are enforced along the top and sides of the cylinder. Of course, the acoustic forcing condition is implemented on the plane at $z = 0$ and begins at time zero. This cylinder is quite large, so the time step for the explicit computer code is quite large. The Reynolds number for this configuration is about 500,000, so the flow field is likely to be turbulent. Note that flow fields possessing Reynolds number exceeding 2000 are expected to exhibit turbulence.[2] Still, for comparison with the configuration to be described in the next subsection, we are using the laminar flow equations. Mixing processes for this model are driven by viscous hydrodynamics.

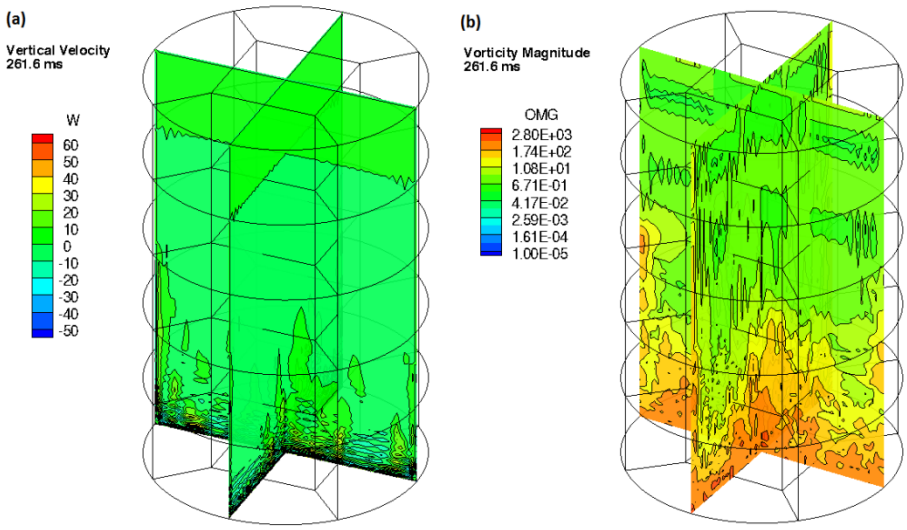

Figure 3. Slices of (a) vertical velocity and (b) vorticity magnitude for the Oxygen-Nitrogen mixing test case at 261.6 ms

For this test case, LESLIE3D executes rather quickly with a time step of about 10^{-5} seconds. In Figure 3, we show plots of vertical velocity and vorticity magnitude at a solution time of 261.6 ms. In Figure 3(a), fluctuations in vertical velocity near the base of the cylinder clearly show the presence of the continuous acoustic wave. A reflection from the top of the mixer is also visible. Perturbations in velocity also appear to crawl up the walls of the cylinder and into the core region. Satisfying the no-slip boundary condition generates vorticity at the base of the cylinder and along the walls. In fact, vorticity develops rather quickly even in the core of the cylinder creating an active mixing environment. Figure 4 exhibits plots of the same properties at 854.6 ms. By this time in the solution process, velocity perturbations have moved completely up the cylinder walls establishing motion throughout the gas. This behavior is evident in Figure 4(a). Figure 4(b) establishes that strong vorticity fluctuations have been established throughout the cylinder. We can conclude that the flow field is being effectively mixed by acoustic forcing. The extent of mixing may also be illustrated by examining a sequence of snapshots of the mass fraction field. Mass fraction plots for gas mixture are shown in Figures 5 and 6. In the course of mixing, it is interesting to observe the Oxygen move upward along the

walls to the top of the mixer. Then it makes its way downward into the core. By the end of the first second, the Nitrogen and Oxygen masses have largely inundated one another. At this rate, thorough mixing is expected within two to three seconds. The maximum temperature exhibited during the first second about 306ºK. In Figures 5 and 6, we have again used slices cast along the *xz* and *yz* planes. The block edges have been removed from the plots for clarity.

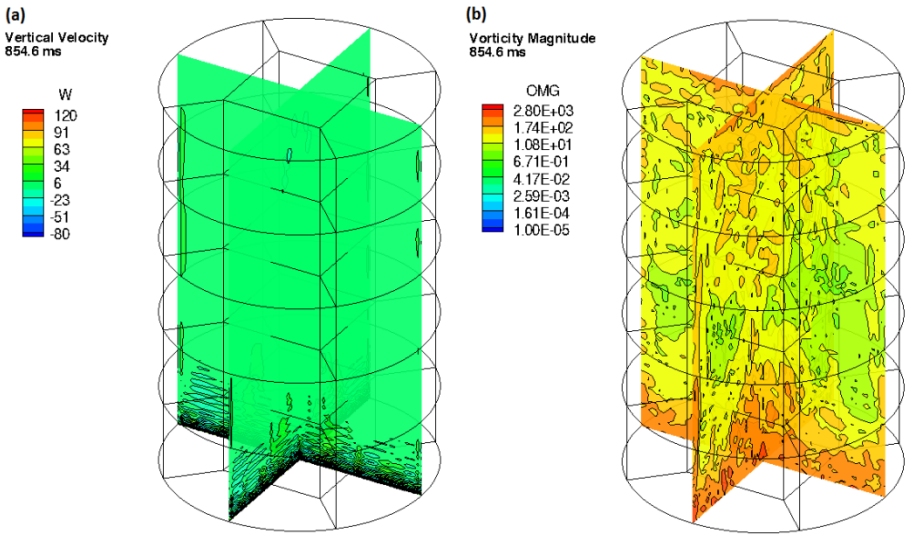

Figure 4. Slices of (a) vertical velocity and (b) vorticity magnitude for the Oxygen-Nitrogen mixing test case at 854.6 ms

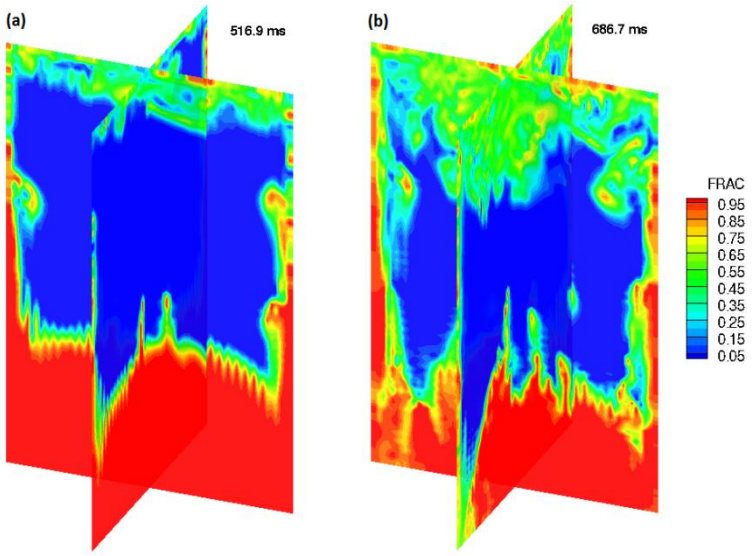

Figure 5. Slices of mass fraction for Oxygen (red) and Nitrogen (blue) at (a) 516.9 ms and (b) 686.7 ms

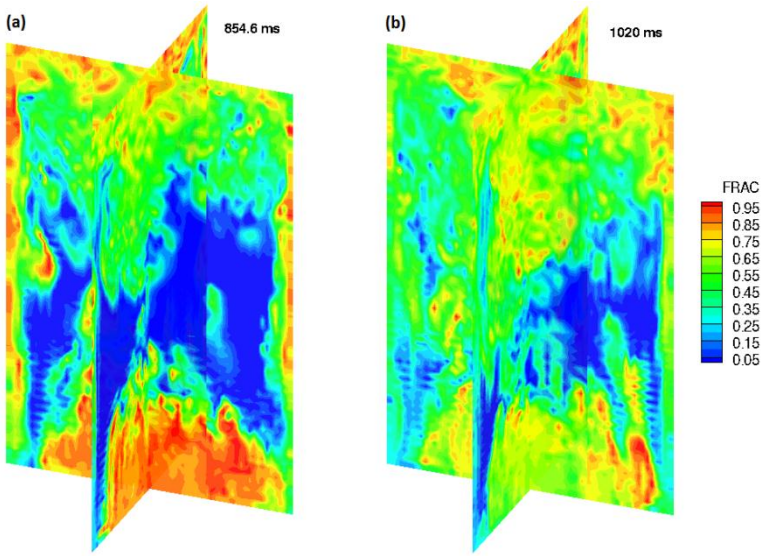

Figure 6. Slices of mass fraction for Oxygen (red) and Nitrogen (blue) at (a) 854.6 ms and (b) 1020 ms

3.2 High Viscosity Mixing

The end goal of a series of numerical studies (this study being the first in the series) is to develop a procedure for simulating the mixing physics for high viscosity materials. Until work began on this project, our experience was limited to the mixing of gases, particles and droplets in turbulent, shocked environments at high Reynolds numbers. Mixing high viscosity materials is a more down to earth project, but it presents significant challenges for LESLIE3D since high viscosity materials attenuate acoustic radiation and delay the destabilization of the two-fluids interface. Investigating methods of operating LESLIE3D to properly capture this type of mixing is an ongoing effort. The results shown below are preliminary.

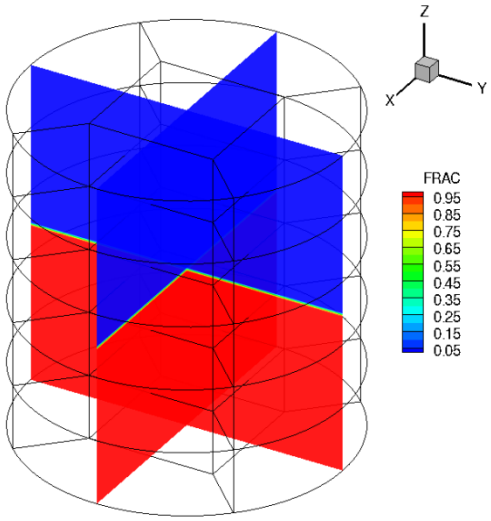

Figure 7. Grid volumes and initial mass fraction distribution for the high viscosity mixing configuration

The high viscosity mixing configuration is shown in Figure 7. The mixing chamber is a cylinder with a height and a diameter of 8.602 cm (3.39 in). The base of the cylinder is located at

z equal zero. The base is also the plane where acoustic excitation is implemented. The cylinder contains two unmixed high viscosity fluids. The interface between the two fluids exists at the cylinder's half height. Both fluids are hydroxyl terminated polybutadienes; at the cylinder top, we have resin R45-HTLO while resin R20-LM resides at the bottom. Estimated properties for these substances are conveyed in Table 1. In most case, for properties such as specific heat and heat of formation, exact values are presently unavailable; reasonable substitutes are made from contemporary literature.[12,13,14] For the results that follow, these properties are assumed to remain constant (no variation with changing temperature). Since this simulation involves no chemical reactions, these results are not sensitive to the heats of formation.

Table 1. Thermophysical, thermochemical and transport properties for high viscosity resins

Resin	Mol. Weight (g/mol)	Viscosity (mPa.s)	Thermal Cond. (W/K/m)	C_p (J/kg/K)	Heat of Form. (J/kg/K)
R45-HTLO	2800	5000	0.1	52.63	54.40
R20-LM	1400	1400	0.1	52.63	90.67

By using LESLIE3D, this test case is simulated for a problem time of about one-third second. Even on 25 processors, this configuration requires a significant amount of computer time. The temporal stepsize is one order of 10^{-7} seconds. The Reynolds number for this configuration is less than one, consistent with a laminar flow field. Plots of (a) vertical velocity and (b) vorticity magnitude at solution time 9.731 ms are shown in Figure 8. MKS units are used

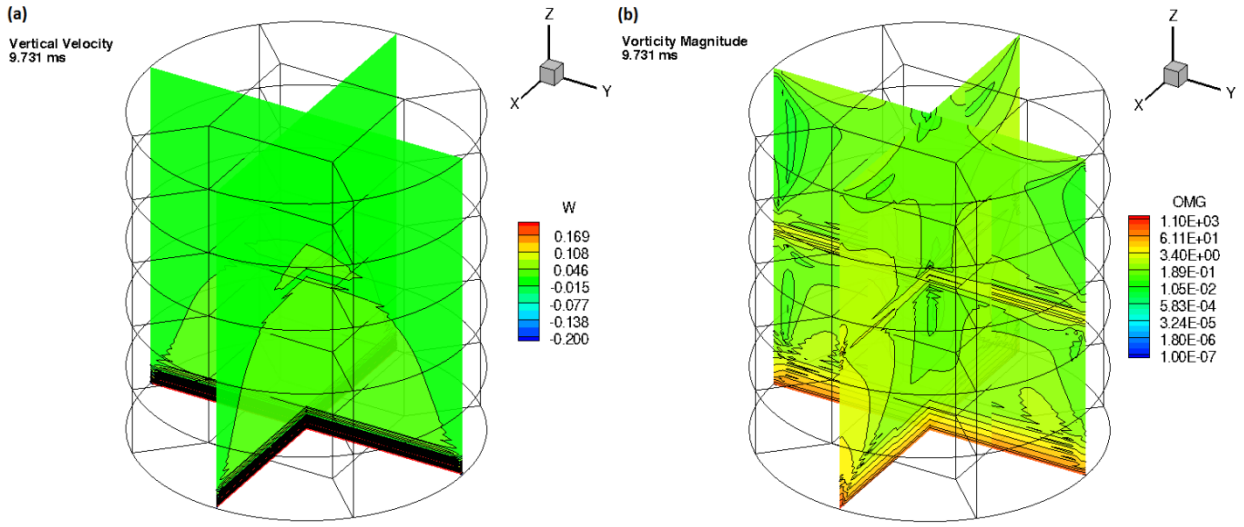

Figure 8. Plots of (a) vertical velocity and (b) vorticity magnitude for the high viscosity mixing problem at 9.731 ms

for all plots. It is evident from Figure 8 that acoustic oscillations attenuate rapidly in the highly viscous fluid. Velocity fluctuations deplete to a tenth of their starting magnitude before traveling half the cylinder's height. Still, the effect of the forcing is felt throughout the cylinder. Vorticity inundates the cylinder volume greatly because of the velocity combined with the requirement for satisfying the no-slip condition along the walls. Similar plots are shown for 73.95 ms in Figure 9.

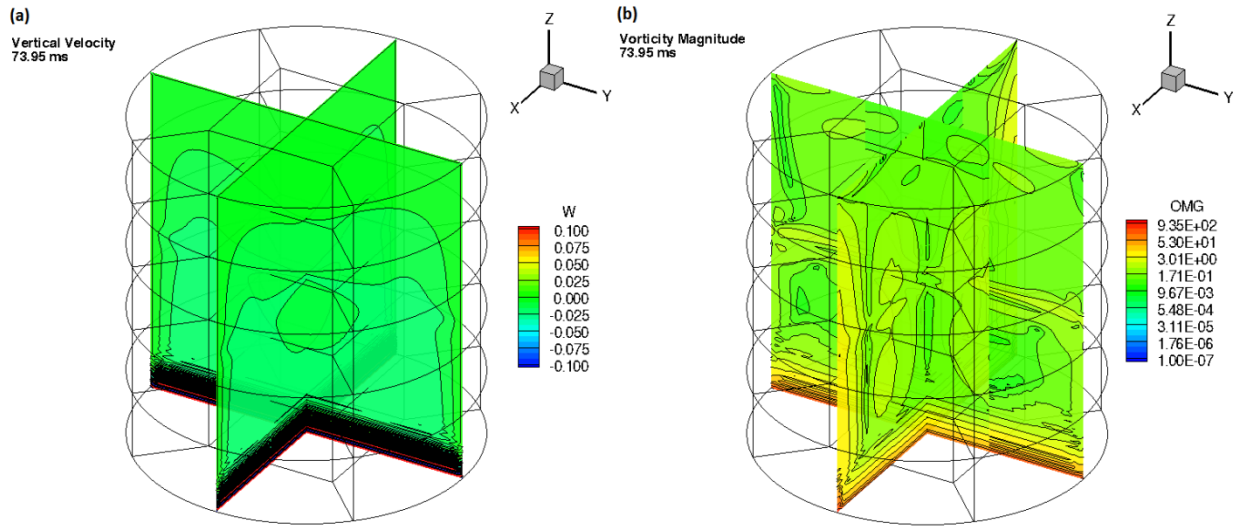

Figure 9. Plots of (a) vertical velocity and (b) vorticity magnitude for the high viscosity mixing problem at 73.95 ms

In Figure 9, the velocity field strengthens on the whole throughout the volume maintaining the level of vorticity through the mixer. The high vorticity bubble can be observed to move along the walls higher into the cylinder. Eddies, regions of circulation, begin to organize within the volume. Figure 10 contains similar information cast at 381.9 ms. At this time, fluid velocity is

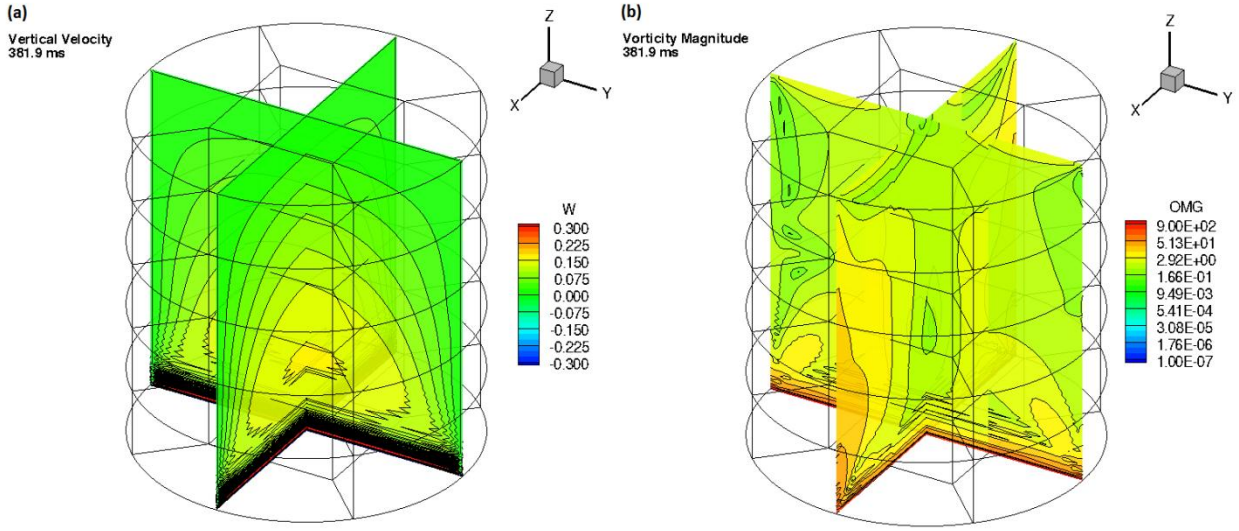

Figure 10. Plots of (a) vertical velocity and (b) vorticity magnitude for the high viscosity mixing problem at 381.9ms

well organized within the mixer and peaks strongly along the central axis. Vorticity fluctuations are becoming very strong along the walls. We expect to see a reasonably high level of perturbation of the interface between the two fluids. This interface is shown in Figure 11. As one

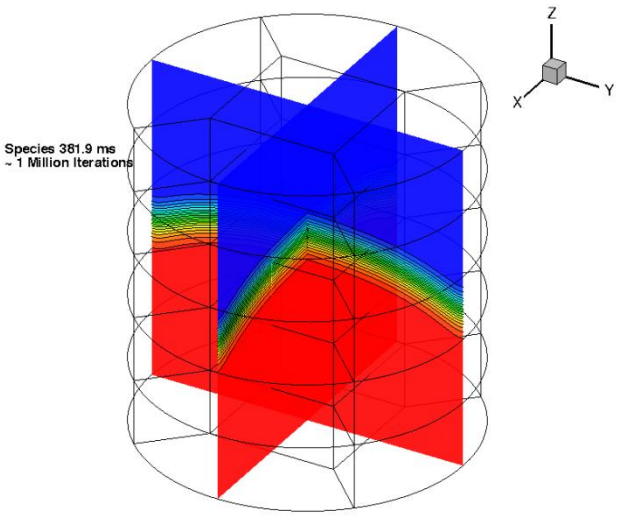

Figure 11. Mass fraction plot for the high viscosity mixing problem at 381.9 ms

may suspect, the interface is spreading due to molecular diffusion and possesses a domed shape because of acoustic forcing. Also, the mass fraction contours are beginning to curl along the wall surfaces, an additional indicator of mixing potential. Yet, at the time this report is written, destabilization of the interface is not observed. As it is in the case of many other physical configurations presented as "new" to a computer code, this simulation is not without its difficulties. The primary difficulty encountered is an issue that we will refer to as overheating. In order to cause mixing, we inundate the flow field near the cylinder base with a strong, continuous acoustic wave. This oscillatory pressure wave creates strong density and temperature fluctuations. In the course of the simulation, temperature builds to an excessive level near the cylinder base. Molecular diffusion cannot remove heat from this area rapidly enough, so unrealistically high temperatures are achieved. This difficulty may be caused by an inadequacy of the equation of state, by an incorrect thermal conductivity value, or perhaps the acoustic excitation model should be cast in terms of a velocity boundary condition. A simple fix being tested now is to implement a non-constant wall temperature model at the cylinder base. This model has the ability to allow heat to escape from the base maintaining the temperature lower. So far, this fix has proven effective.

Other issues deal with the transport model. In truth, viscosity is a function of temperature. For liquids or soft solids, we expect viscosity to fall with rising temperature. This aspect of physics is not incorporated in the present model. Enough data does exist to build a temperature dependent model in the future, and it is not difficult to enter this type of model into LESLIE3D. Another potential issue lies in the initiation of the hydrodynamic instability at the material interface. In the Oxygen-Nitrogen model, this instability tripped on its own, probably due to a tiny grid irregularity located at interface between two blocks. So far for this case, we have not seen the flow instability trip perhaps due to the effects of high viscosity. This instability is the event that initiates realistic mixing. For the high viscosity model, it may be necessary to perturb the flow field at the material interface to initiate mixing. This type of perturbation is not difficult to implant within the problem, yet this change must be made with care. It is also important to remember that this problem is being solved by algorithms for gas dynamics, and gravity is not implemented. It follows that there will be some aspects of table-top RAM mixing that the

computer code cannot easily mimic. An example is that of a void above the material. In gas dynamics, we do not usually expect to see true voids in a slow speed flow solution. In general, we must fill the field with non-zero density gas everywhere. When mixing liquids or solids, the RAM does not have this limitation. In the long run, it is desirable to modify LESLIE3D to model RAM's physics more closely, but for now, LESLIE3D is a serviceable tool for studying the process of RAM.

4.0 CONCLUSIONS

This technical report concentrates on studying the dynamics associated with Resonant Acoustic Mixing (RAM). This process involves the use of continuous wave acoustic signals (or vibrations) to mix materials by exploiting an interesting coupling between pressure and vorticity fluctuations. LESLIE3D, a parallel, multiphase physics computer program developed by the Georgia Institute of Technology is the tool applied to simulate two basic mixing cases. The theory behind LESLIE3D is discussed in this report focusing primarily on low Reynolds number flow fields. Also, the algorithm used to implement acoustic excitation in LESLIE3D is presented, and its inner workings are contrasted with some available information on the functioning of the resonant acoustic mixer. Two test cases are addressed in the report. The first is the mixing of Oxygen and Nitrogen. This test case is simple to implement and results in fully developed mixing. Much information on the fluid dynamics of mixing can be extracted from this test case. The second test case addresses our target application. Here, the problem of mixing two highly viscous resins is tackled. This simulation, although incomplete, generates a realistic velocity field and deforms the material interface in a realistic manner. The purpose of this test case is to educate the researcher on how to solve this type of problem using the computer code. We have detected difficulties in overheating near the acoustic boundary, and we may have determined a potential need for manually "tripping" the instability that initiates mixing. Still, the high viscosity mixing problem remains under investigation.

In the future, we plan to incorporate particles within the flow field, a step closer to the target application of this simulation technique. Also, a series of simple one or two component mixing problems are to be solved for comparison with experiment. It is desirable to see whether or not, with limitations in hand, that LESLIE3D can mimic the basic mechanism of mixing observed for resins. The acoustic boundary condition may also be modified in order to improve the way it performance in comparison with the laboratory mixer. We may also extend the size of the simulation for massively parallel execution.

REFERENCES

1. ResonantAcoustic® Mixing, Resodyne Acoustic Mixers, Butte, Montana, 2013, pp. 1-8.

2. Schlicting, H., *Boundary Layer Theory*, 7th Ed., McGraw-Hill, Inc., New York, 1979.

3. Richtmyer, R.D., "Taylor instability in shock acceleration of compressible fluids", *Communications in Pure and Applied Mathematics*, Vol. 13, 1960, pp. 297-319.

4. Pope, S.B., *Turbulent Flows*, Cambridge University Press, New York, 2000.

5. Lee, S. and Kim, J., "Prediction of rotor high-speed impulsive noise with a combined CFD-Kirchhoff method", *Journal of Sound and Vibration*,Vol. 207, No. 4, 1997, pp. 453-464.

6. Hirsch, C., *Numerical Computation of Internal and External Flows*, John Wiley & Sons, New York, 1990.

7. Sedov, L.I., *Similarity and Dimensional Methods in Mechanics*, 10th Ed., CRC Press, Boca Raton, 2000.

8. Menon, S., "Active combustion control in a ramjet using large-eddy simulations", *Combustion Science and Technology*, Vol. 84, 1992, pp. 51-79.

9. Burden, R.L., Faires, J.D. and Reynolds, A.C., *Numerical Analysis*, 2nd Ed., Prindle, Weber & Schmidt, Boston, MA, 1981.

10. MacCormack, R.W., "The effect of viscosity in hypervelocity impact cratering", *Journal of Spacecraft and Rockets*, Vol. 40, No. 5, 2003, pp. 757-763.

11. Poinsot, T.J. and Lele, S.K., "Boundary conditions for direct simulations of compressible viscous flows", *Journal of Computational Physics*, Vol. 101, 1992, pp. 104-129.

12. Rajesh, K.K, "Thrust modulation is a nitrous-oxide/hydroxyl-terminated polybutadiene hybrid rocket motor", AIAA 2006-4503, 42nd AIAA/ASME/SAE/ASEE Joint Propulsion Conference & Exhibit, Sacramento, CA, 2006.

13. Grebowicz, J., Aycock, W. and Wunderlich, B., "Heat capacities of 1,4-polybutadienes", *Polymer*, Vol. 27, 1986, pp. 575-582.

14. Hydroxyl Terminated Polybutadiene Resins and Derivatives – Poly bd and Krasol, Product Bulletin, Sartomer Company, Inc., Exton, PA, 2013.

LIST OF ACRONYMS, ABBREVIATIONS, AND SYMBOLS

This section contains brief definitions of various terms and acronyms used throughout this document. Only terms and acronyms whose definitions are considered uncommon are included.

C_p - Constant pressure specific heat
C_v - Constant volume specific heat
D_m - Diffusion coefficient for species *m*
E - Total energy per unit mass
e - Specific internal energy
h_m - Enthalpy of species *m*
K - Heat conduction coefficient
P - Thermodynamic pressure (absolute)
q_i - i^{th} component of heat conduction vector (Fourier's Law)
R - Species perfect gas constant
T - Absolute temperature
t - Time coordinate
u_i - i^{th} Cartesian velocity component
V_{im} - i^{th} Cartesian component of diffusion velocity for species *m*
x_i - i^{th} Cartesian space coordinate
Y_m - Mass fraction of chemical species *m*

γ - Ratio of specific heats
Δh^0_{fm} - Heat of formation for species *m*
δ_{ij} - Dirac delta
λ - Stoke's parameter
μ - Dynamic viscosity
ρ - Mixture density
τ_{ij} - Shear stress tensor
$\dot{\omega}_m$ - Production rate for species *m*
Θ - Dimensionless temperature

DISTRIBUTION LIST
AFRL-RW-EG-TR-2013-079

Defense Technical Information Center Attn: Acquisition (OCA) 8725 John J. Kingman Road, Ste 0944 Ft Belvoir, VA 22060-6218	1 Electronic Copy (1 file, 1 format)

EGLIN AFB OFFICES:

AFRL/RWOC (STINFO Tech Library Copy)	1 Copy
AFRL/RW CA-N	Notice of publication only
AFRL/RWMES	1 Copy